Quantitative Transport Measurements of Fractional Quantum Hall Energy Gaps in Edgeless Graphene Devices

H. Polshyn,[1] H. Zhou,[1] E. M. Spanton,[1] T. Taniguchi,[2] K. Watanabe,[2] and A. F. Young[1]
[1]*Department of Physics, University of California, Santa Barbara, California 93106, USA*
[2]*Advanced Materials Laboratory, National Institute for Materials Science, Tsukuba, Ibaraki 305-0044, Japan*

(Received 28 August 2018; revised manuscript received 19 October 2018; published 28 November 2018)

Owing to their wide tunability, multiple internal degrees of freedom, and low disorder, graphene heterostructures are emerging as a promising experimental platform for fractional quantum Hall (FQH) studies. Here, we report FQH thermal activation gap measurements in dual graphite-gated monolayer graphene devices fabricated in an edgeless Corbino geometry. In devices with substrate-induced sublattice splitting, we find a tunable crossover between single- and multicomponent FQH states in the zero energy Landau level. Activation gaps in the single-component regime show excellent agreement with numerical calculations using a single broadening parameter $\Gamma \approx 7.2$ K. In the first excited Landau level, in contrast, FQH gaps are strongly influenced by Landau level mixing, and we observe an unexpected valley-ordered state at integer filling $\nu = -4$.

DOI: 10.1103/PhysRevLett.121.226801

Advances in graphene sample fabrication [1–6] now allow a wide range of fractional quantum Hall (FQH) states to be accessed experimentally [6–18]. Understanding these phases is complicated by the near degeneracy of different components of the combined spin and valley isospin. Interaction-driven mixing of different isospin components manifests as strong violations of particle-hole (PH) symmetry across individual Landau levels (LLs) [9,10,15] and multiple B-tuned phase transitions between FQH states with differing isospin polarizations [11,18]. However, the isospin degeneracy enlarges the Hilbert space available for constructing FQH ground states, rendering full numerical treatment of the system prohibitively expensive computationally. Historically, thermally activated transport measurements have played a critical role in deconvolving the role of internal degrees of freedom in other FQH systems. Unfortunately, however, the exceptional quality of the graphene bulk observed in capacitance measurements does not manifest clearly in electronic transport [6,17], precluding detailed studies of FQH gaps in the highest quality samples.

In this Letter, we report the fabrication of samples that combine edge-free Corbino topology [19–22] with hexagonal boron nitride (hBN) encapsulation [5] and dual graphite gating [6]. We study two devices showing a large sublattice asymmetry gap (Δ_{AB}) that removes the valley degree of freedom—equivalent to sublattice in the zero Landau level (ZLL)—at low magnetic fields [23]. We map out the competition between single- and two-component fractional quantum Hall physics in both the spin and valley sectors and find a single-component regime where FQH gaps can be quantitatively compared to exact diagonalization calculations. From the resulting analysis, we assess the degree of disorder in graphene devices, which we find to be only a few times higher than in high mobility GaAs quantum wells [24]. Finally, we use these devices to explore the first excited LL (FLL) in detail, finding evidence for asymmetric LL mixing and discovering an unexpected valley-ordered (VO) state at half filling of this fourfold degenerate level.

Our fabrication process begins with a dry-transferred van der Waals heterostructure [5] comprising a graphene sheet sandwiched between two graphite gates and two hBN spacer layers. A Corbino topology device is then fabricated through a variety of lithography, etching, and—crucially—a sublimation-based stack inversion step that allows patterning of aligned holes in the top and bottom gates without contamination of critical dielectric interfaces. The fabrication process is depicted schematically in Fig. 1(a) and detailed in Ref. [25]. Integer quantum Hall features emerge at $B \lesssim 50$ mT [Fig. 1(c)], indicating high sample quality. We focus on two samples, both of which show thermally activated transport [Fig. 1(d)] at charge neutrality and zero magnetic field, which previous work [23,26] has tied to a substrate-induced staggered sublattice potential Δ_{AB}. We estimate the magnitude $\Delta_{AB} \approx 10$–20 meV in the two devices based on fits to an Arrhenius law and on the width of the insulating state in gate voltage (Fig. S2 of Supplemental Material [25]). Within the ZLL, Δ_{AB} translates directly to a splitting between the two valley-polarized Landau levels.

In the ZLL, mixing with other orbital LLs is weak. Individual isospin-polarized LLs would naively be expected to show particle-hole symmetry, defined as equivalence between FQH states at LL filling factors ν and $-1-\nu$ (here, $\nu = 2\pi\ell_B^2 n$, with n the charge density and $\ell_B \approx 25.7\ \text{nm}\sqrt{B_\perp[\text{T}]}$ the magnetic length). However, PH asymmetry can arise when two or more isospin components

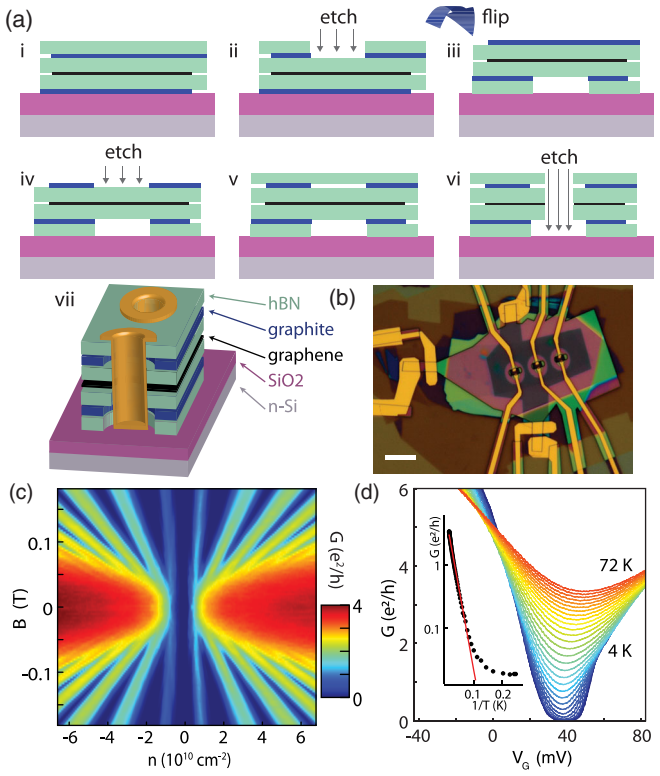

FIG. 1. Edgeless graphene devices. (a) Steps for fabricating internal contacts. (i) Dry transfer produces a hBN/graphite/hBN/graphene/hBN/graphite heterostructure. (ii) A hole is etched in the top hBN and first graphite layer. (iii) The stack is flipped upside down, exposing the second graphite layer. (iv) The exposed graphite is etched and (v) another hBN flake deposited. (vi) A hole is etched through the entire stack to expose the graphene for (vii) edge contacting [5]. (b) Optical micrograph of device A. Scale bar is 10 μm. (c) Conductance of device B at low magnetic fields. The insulating state persisting through $B = 0$ at charge neutrality is associated with broken AB sublattice symmetry [23,26]. (d) Thermally activated transport at charge neutrality in device A. The measured activation gap $\Delta_{AB} \approx 114$ K.

are close in energy. In this case, filling factors related by a PH transformation may host different multicomponent wave functions or allow different low energy excitations to other spin or valley branches, resulting in contrasting thermal activation gaps and absence of PH symmetry. Single-component physics obtains only when ground states involve only a single isospin projection, and the low-lying thermal excitations do not involve isospin reversals. The role of internal degeneracy in two-component FQH systems is controlled by the ratio between the single-particle splitting of that degeneracy and the Coulomb energy [$E_C = e^2/(\epsilon \ell_B) \approx 8.5\ \mathrm{meV}\sqrt{B_\perp[\mathrm{T}]}$ using the measured [27] in-plane dielectric constant of the encapsulating hBN layers $\epsilon = 6.6$]. Theoretical calculations [28] suggest that multicomponent physics is relevant in the FQH regime only when LL separations are smaller than $0.05E_C$, with the precise threshold strongly dependent on the filling factor.

Figures 2(a)–2(c) show transport measurements for device A taken at $B_\perp = 18$, 14, and 3 T for $\nu \in (0, -1)$. Both the highest and lowest magnetic field traces are PH asymmetric across the single Landau level, reflected in asymmetric conductivity minima within the $\nu = p/(2p \pm 1)$ ($p \in \mathbb{Z}$) sequence of FQH states. At $B = 18$ T, PH asymmetry is accompanied by a well-developed insulating state at $\nu = -1/2$. A similar breakdown of PH symmetry and even-denominator incompressible state was recently reported [18]. Both phenoma arise due to a crossing between LLs in opposite valleys, driven by competition between Δ_{AB} (which is $B_\perp$ independent) and an intrinsic antiferromagnetic anisotropy that grows with $B_\perp$. Figure 2(d) shows a schematic representation of the resulting LL energies. The spin- and sublattice-polarized $|A\downarrow\rangle$LL, relevant for fillings $\nu \in (0, -1)$, is depicted in red. Multicomponent physics is expected when other LLs come within $\approx 0.05E_C$ of this level, corresponding to the shaded region.

In the high $B_\perp$ regime Coulomb interactions thus mix the $|A\downarrow\rangle$ and $|B\downarrow\rangle$LLs leading to multicomponent FQH ground states and excitations between the two sublattices [18]. At lower B field FQH states are fully polarized on one sublattice. Multicomponent physics can nevertheless arise from mixing between spin branches, which are split only by the bare Zeeman energy $E_Z \approx 0.115\ \mathrm{meV} \times B_T[\mathrm{T}]$. Indeed, at the lowest magnetic fields of 3 T, we estimate that $E_Z = 0.023E_C$, well below the threshold for multicomponent physics [28].

In order to address the role of spin quantitatively, we measure thermal activation gaps ${}^{\nu}\Delta$ in this regime as a function of B_T. ${}^{\nu}\Delta$ measures the energy of the lowest energy charged excitation at filling ν, which for a single-component system is a quasiparticle-quasihole pair but in multicomponent systems can consist of charged spin textures. Figure 2(e) shows the evolution with B_T of the $\nu = -1/3$, $-2/3$, $-4/3$, and $-5/3$ gaps at $B_\perp = 4$ T. While the $\nu = -1/3$ and $-5/3$ gaps are independent of in-plane magnetic field, the $\nu = -2/3$ and $-4/3$ gaps grow rapidly with B_T, consistent with spin-reversed charged excitations [29]. For $B_T \gtrsim B_T^* \approx 6.4$ T, corresponding to $\kappa \gtrsim 0.043$, all four gaps are equal within experimental error and particle-hole symmetry is restored.

The behavior at all $n/3$ fillings can be qualitatively understood within a composite fermion (CF) model [31], sketched in Fig. 2(f). In the CF picture, interacting electrons at partial LL filling are considered as *noninteracting* states of composite particles consisting of an electron and two magnetic flux quanta. CFs experience an effective magnetic field $B_{\mathrm{eff}} = B_\perp(1 - 2\nu)$, leading to integer filling p of CF LLs (termed Λ levels) at electron filling $\nu = p/(2p \pm 1)$. For simplicity, we count electronic states relative to the $\nu = -2$ vacuum state. The $-5/3$ state corresponds to filling a single Λ level, while the $-4/3$ consists of filling two Λ levels. In a two-component system, the $-1/3$ ($-2/3$) state

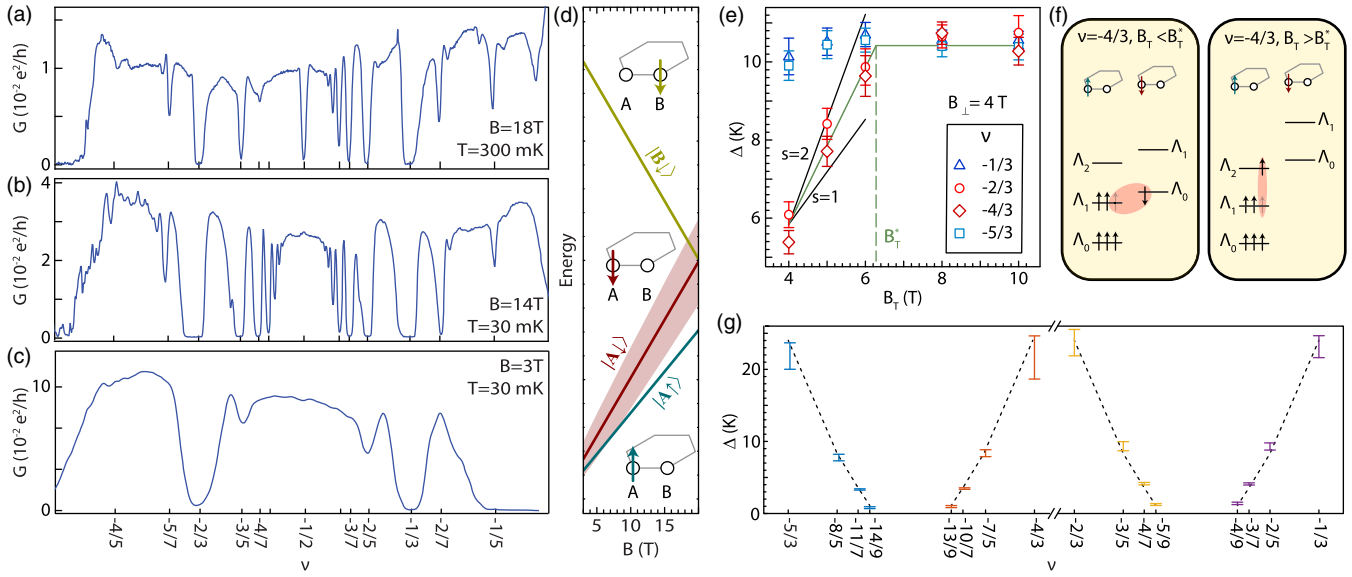

FIG. 2. Fractional quantum Hall gaps in the zero energy Landau level. (a)–(c) Magnetotransport data from device A at (a) $B_\perp = B_T = 18$ T (b) 14 T, and (c) 3 T. (d) LL energy diagram in gapped monolayer graphene. The shaded region around the $|A\downarrow\rangle$LL indicates energy intervals of $\pm 0.05 E_C$; single component physics for $\nu \in (-1, 0)$ is expected only when no other LLs are within this range. At low $B_\perp$, Coulomb interactions mix this level with the $|A\uparrow\rangle$LL, while at high $B_\perp$ growing antiferromagnetic anisotropy leads to another LL crossing and mixing with the $|B\downarrow\rangle$LL [18]. (e) B_T dependence of $n/3$ activation gaps for $B_\perp = 4$ T. The gaps at $-2/3$ and $-4/3$ grow with B_T below $B_T^* \approx 6.4$ T before saturating. Black lines indicate expected slope for spin-flip excitations involving $s = 1$ and $s = 2$ flipped spins [29]. (f) Λ level energy diagram for $\nu = -4/3$. For $B_T < B_T^*$; the polarized $-4/3$ state has low energy excitations consisting of spin-reversed particle-hole pairs, while for $B_T > B_T^*$ state admits only spinless particle-hole excitations. (g) FQH activation gaps in device A at $B_\perp/B_T = 10$ T/14 T. Dashed lines are numerical results for a single-component system [30] with a constant phenomenological broadening $\Gamma = 7.2$ K subtracted.

is related to the $-5/3$ ($-4/3$) state by particle-hole symmetry across the two-component LL, $\nu \leftrightarrow -2 - \nu$.

In this picture, the Zeeman energy at $B_\perp/B_T = 4\text{T}/4\text{T}$ is sufficient to spin polarize the $-4/3$ and $-2/3$ ground states, but small enough that the low energy excitations are nevertheless spin flips [32,33]. At $\nu = -5/3$, only one level is filled in the same diagram, and spin-flip excitations are not favored even at the lowest values of B_T probed. For $B_T > B_T^*$, however, the increased Zeeman energy makes the spin-flip excitation energetically unfavorable even at $-2/3$, resulting in a crossover to a conventional inter-Λ level excitation without a reversed spin and a transition between two-component and single-component FQH physics.

Our observations are consistent with exact numerical simulations for two-component FQH systems [34], which predict that spin-flip excitations are relevant at $\nu = -1/3$ only for $E_Z < 0.009 E_C$ ($B_\perp = B_T < 0.44$ T in our devices). Similar calculations suggest that a spin-unpolarized $2/3$ state should obtain only for $\kappa < 0.017$ [28,35], corresponding to $B_\perp = B_T < 1.8$ T in our devices—just below the regime where the $2/3$ state develops in our samples. Finally, residual interactions between composite fermions complicate the schematic picture of Fig. 2(f): spin-flip excitations themselves can involve multiple spins, which manifest in the B_T dependence of energy gaps as $\partial\Delta/\partial B_T = sg\mu_B$, where s corresponds to the number of flipped spins [29]. We find that $s > 1$ see Fig. 2(e)], suggesting that excitations at $\nu = -2/3$ and $-4/3$ are extended spin textures rather than single reversed spins. The detailed nature of spin excitations at $\nu = 2/3$ has only begun to be addressed numerically [36].

To access a single-component regime of FQH in graphene, one needs a Zeeman energy sufficiently strong to prevent spin-flip excitations, but $B_\perp$ sufficiently weak to avoid multicomponent valley physics arising from the $B_\perp$-tuned valley level crossing reported in Ref. [18]. Figure 2(g) shows thermal activation gaps for a range of fractional fillings at $B_\perp = 10$ T and $B_T = 14$ T, well within this regime. The energy gaps are PH symmetric across all four individual isospin resolved LLs, as expected for single-component FQH systems. Indeed, our measured FQH gaps are well matched to exact diagonalization calculations [30] using only a single phenomenological LL broadening parameter, Γ, to capture the effects of disorder, so that ${}^\nu\Delta_{\text{meas}} = {}^\nu\Delta_{ED} - \Gamma$. All four series of gaps within the ZLL are well fit by $\Gamma = 7.2$ K. For comparison, similar analysis on a GaAs 2DEG of mobility 7×10^6 cm^2/(V s) found $\Gamma = 2$ K from fitting the behavior of the $1/3$ state [24]. Restriction of FQH excitations to a single spin component is further supported by the absence of any dependence on B_T, with gaps at $B_\perp = 10$ T, $B_T = 14$ T equal to those

measured at $B_\perp = B_T = 10$ T within experimental error, consistent with the second spin branch remaining inert. We note that in systems with $\Delta_{AB} = 0$ [9,10], a single-component regime is not accessible as the valleys are always degenerate at the single-particle level, so that low-lying FQH excitations at some ν will always involve intervalley excitations.

The first excited LL, spanning $-6 < \nu < -2$, also shows robust FQH sequences [Fig. 3(a)]. Activation gaps, although similarly Zeeman energy independent [see Figs. S3(e) and S3(f) [25]], diverge sharply from those in ZLL [Fig. 2(g)]. Most prominently, FQH gaps are strongly PH asymmetric even across the entire quartet LL, i.e., ${}^{\nu}\Delta \neq {}^{-8-\nu}\Delta$. This asymmetry indicates that mixing with the ZLL and second excited level plays an important role in determining activation gaps. In this picture, FQH states in the FLL at high $|\nu|$ mix more heavily with higher LLs, whose orbital structure is less favorable to FQH states. Because applicable numerical simulations are not available, we analyze the data using a noninteracting composite fermion picture. The CF picture predicts a linear dependence of the energy gaps on ν within each FQH series, a trend well matched by the data, and allows us to quantify trends in ν across the level. In addition to the broadening Γ defined above, linear fits are parametrized by a phenomenological composite fermion cyclotron mass $m_{\rm cyc}$ such that $\Delta_{\rm meas} = (\hbar e B_{\rm eff}/m_{\rm cyc}) - \Gamma$. Figures 3(c) and 3(d) show the result of such fits across the LL.

We also find a new phase at integer filling $\nu = -4$, corresponding to half filling of the first excited LL. Figures 4(a) and 4(b) shows low $B_\perp$ measurements in the first excited LL, with a phase transition at $B_\perp \approx 2.3$ T evident as a rise in conductivity at $\nu = -4$ separating distinct low- and high-B insulating states. Increasing B_T by tilting the field strengthens the high-$B_\perp$ state, suggesting that it is spin polarized (SP) while the low-$B_\perp$ insulator is a spin-unpolarized, and consequently VO, quantum Hall ferromagnetic state [Fig. 4(c)]. The transition can be understood phenomenologically by competition between the spin Zeeman effect and a valley splitting Δ_V, with the transition occurring when $\Delta_V = E_Z$, allowing us to estimate $\Delta_V \approx 3$ K [Fig. 4(d)].

The origin of Δ_V is unclear. While a sublattice gap Δ_{AB} generates a large single-particle splitting between valleys in the ZLL, it generates only a small splitting $\Delta_V \ll 1$ K in the 1LL. It is instructive to compare the competition between the phases at $\nu = -4$ with small Δ_V with the competition between phases at $\nu = 0$ in samples with $\Delta_{AB} \approx 0$. In the latter case, the anisotropy of the Coulomb interactions on the lattice scale [37,38] chooses between a set of nearly degenerate isospin polarized states. The resulting antiferromagnetic ground state can be suppressed in favor of a spin-polarized state by large B_T.

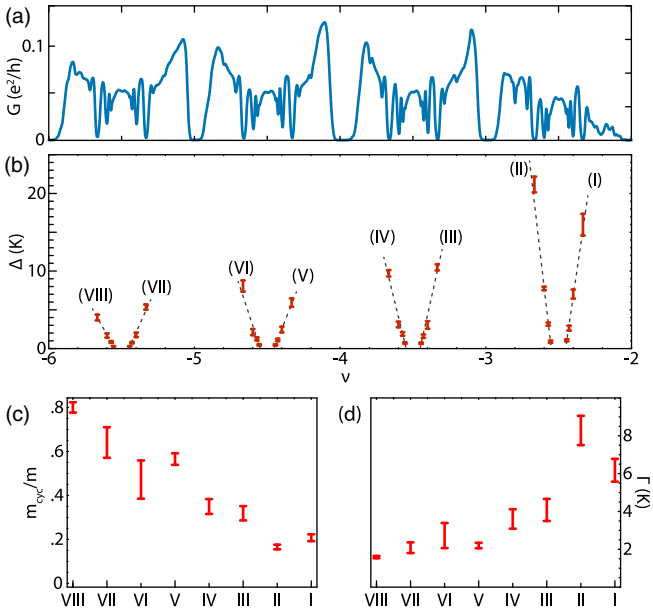

FIG. 3. Fractional and integer quantum Hall gaps in the first excited LL. (a) Conductance of device A measured at $B = 10$ T. (b) Measured FQH activation gaps. Dashed lines are linear fits to the function $\Delta = eB_{\rm eff}/m_{\rm cyc} - \Gamma$ (defined in the main text) for each FQH series labeled by the numerals (I)–(VIII). (c) Composite fermion cyclotron mass $m_{\rm cyc}$ and (d) broadening Γ extracted from \the linear fits for the different FQH series I–VIII in the first excited LL.

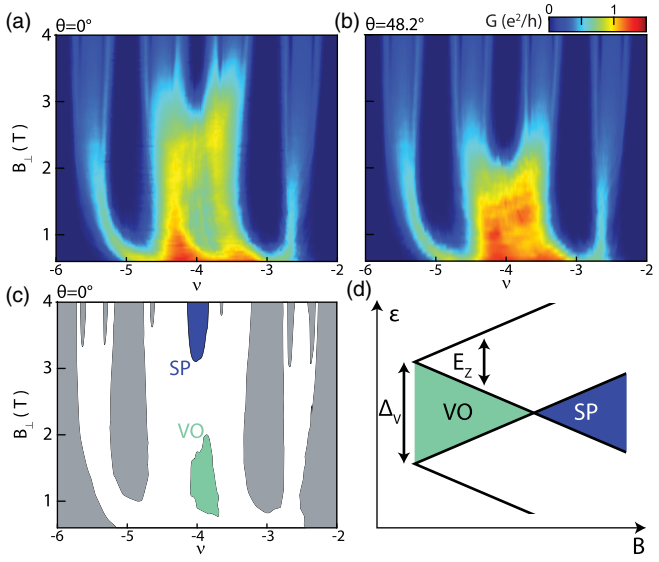

FIG. 4. Valley-ordered (VO) phase at $\nu = -4$ in device B (for device A, see Fig. S4 [25]). (a) Conductance in the first excited Landau level at $B_\perp = B_T$. Two insulating states are visible, at low and high $B_\perp$, noted schematically in (c). (b) Conductance in the first excited LL in tilted field, with $B_\perp = 0.67 B_T$. The low-$B_\perp$ state is suppressed. (d) Level crossing model for the phase transition. A VO state driven by a valley splitting Δ_V (which may have either single-particle or many-body origin) is suppressed by the Zeeman splitting E_Z, which favors a spin-polarized (SP) state.

Determining the nature of the low-B insulating state at $\nu = -4$ may involve a similarly subtle interplay of anisotropies, with Δ_V having either single-particle or many-body origin.

In conclusion, we have introduced a versatile fabrication method for producing van der Waals heterostructure devices in which measured transport occurs entirely through the sample bulk. We use sublattice and Zeeman splittings to access a single-component FQH regime, and activation gap measurements to quantify the LL broadening. We find that graphite-gated graphene 2D electron systems are comparable to high mobility GaAs quantum wells. Future experiments may leverage this fabrication technique, for example, to study edge transport in entirely gate-defined devices fabricated in the interior of a single graphene flake.

We thank Cory Dean, S. Chen, Y. Zeng, M. Yankowitz, and J. Li for discussing their unpublished data and for sharing the stack inversion technique. The authors acknowledge further discussions of the results with I. Sodemann, M. Zaletel, C. Nayak, and J. Jain. A. F. Y., H. P., H. Z., and E. M. S. were supported by the ARO under awards 69188PHH and MURI W911NF-17-1-0323. A portion of this work was performed at the National High Magnetic Field Laboratory, which is supported by National Science Foundation Cooperative Agreement No. DMR-1644779 and the State of Florida. K. W. and T. T. acknowledge support from the Elemental Strategy Initiative conducted by the MEXT, Japan, and JSPS KAKENHI Grant No. JP15K21722. E. M. S. acknowledges the support of the Elings Prize Fellowship in Science of the California Nanosystems Institute at the University of California, Santa Barbara. A. F. Y. acknowledges the support of the David and Lucile Packard Foundation.

[1] K. I. Bolotin, K. J. Sikes, Z. Jiang, M. Klima, G. Fudenberg, J. Hone, P. Kim, and H. L. Stormer, Solid State Commun. **146**, 351 (2008).
[2] X. Du, I. Skachko, A. Barker, and E. Y. Andrei, Nat. Nanotechnol. **3**, 491 (2008).
[3] C. R. Dean, A. F. Young, I. Meric, C. Lee, L. Wang, S. Sorgenfrei, K. Watanabe, T. Taniguchi, P. Kim, K. L. Shepard, and J. Hone, Nat. Nanotechnol. **5**, 722 (2010).
[4] A. S. Mayorov, R. V. Gorbachev, S. V. Morozov, L. Britnell, R. Jalil, L. A. Ponomarenko, P. Blake, K. S. Novoselov, K. Watanabe, T. Taniguchi, and A. K. Geim, Nano Lett. **11**, 2396 (2011).
[5] L. Wang, I. Meric, P. Y. Huang, Q. Gao, Y. Gao, H. Tran, T. Taniguchi, K. Watanabe, L. M. Campos, D. A. Muller, J. Guo, P. Kim, J. Hone, K. L. Shepard, and C. R. Dean, Science **342**, 614 (2013).
[6] A. A. Zibrov, C. Kometter, H. Zhou, E. M. Spanton, T. Taniguchi, K. Watanabe, M. P. Zaletel, and A. F. Young, Nature (London) **549**, 360 (2017).
[7] K. I. Bolotin, F. Ghahari, M. D. Shulman, H. L. Stormer, and P. Kim, Nature (London) **462**, 196 (2009).
[8] X. Du, I. Skachko, F. Duerr, A. Luican, and E. Y. Andrei, Nature (London) **462**, 192 (2009).
[9] C. R. Dean, A. F. Young, P. Cadden-Zimansky, L. Wang, H. Ren, K. Watanabe, T. Taniguchi, P. Kim, J. Hone, and K. L. Shepard, Nat. Phys. **7**, 693 (2011).
[10] B. E. Feldman, B. Krauss, J. H. Smet, and A. Yacoby, Science **337**, 1196 (2012).
[11] B. E. Feldman, A. J. Levin, B. Krauss, D. A. Abanin, B. I. Halperin, J. H. Smet, and A. Yacoby, Phys. Rev. Lett. **111**, 076802 (2013).
[12] A. Kou, B. E. Feldman, A. J. Levin, B. I. Halperin, K. Watanabe, T. Taniguchi, and A. Yacoby, Science **345**, 55 (2014).
[13] D.-K. Ki, V. I. Falko, D. A. Abanin, and A. F. Morpurgo, Nano Lett. **14**, 2135 (2014).
[14] P. Maher, L. Wang, Y. Gao, C. Forsythe, T. Taniguchi, K. Watanabe, D. Abanin, Z. Papic, P. Cadden-Zimansky, J. Hone, P. Kim, and C. R. Dean, Science **345**, 61 (2014).
[15] F. Amet, A. J. Bestwick, J. R. Williams, L. Balicas, K. Watanabe, T. Taniguchi, and D. Goldhaber-Gordon, Nat. Commun. **6**, 5838 (2015).
[16] A. J. Bestwick, C.-T. Liang, D. Goldhaber-Gordon, F. Amet, G. Diankov, J. Jaroszynski, K. Watanabe, K. Tharratt, M. Lee, P. Gallagher, T. Taniguchi, and W. Coniglio, Nat. Commun. **7**, 13908 (2016).
[17] J. I. A. Li, C. Tan, S. Chen, Y. Zeng, T. Taniguchi, K. Watanabe, J. Hone, and C. R. Dean, Science **358**, 648 (2017).
[18] A. A. Zibrov, E. M. Spanton, H. Zhou, C. Kometter, T. Taniguchi, K. Watanabe, and A. F. Young, Nat. Phys. **14**, 930 (2018).
[19] J. Yan and M. S. Fuhrer, Nano Lett. **10**, 4521 (2010).
[20] E. C. Peters, A. J. M. Giesbers, M. Burghard, and K. Kern, Appl. Phys. Lett. **104**, 203109 (2014).
[21] Y. Zhao, P. Cadden-Zimansky, F. Ghahari, and P. Kim, Phys. Rev. Lett. **108**, 106804 (2012).
[22] M. J. Zhu, A. V. Kretinin, M. D. Thompson, D. A. Bandurin, S. Hu, G. L. Yu, J. Birkbeck, A. Mishchenko, I. J. Vera-Marun, K. Watanabe, T. Taniguchi, M. Polini, J. R. Prance, K. S. Novoselov, A. K. Geim, and M. Ben Shalom, Nat. Commun. **8**, 14552 (2017).
[23] B. Hunt, J. D. Sanchez-Yamagishi, A. F. Young, M. Yankowitz, B. J. LeRoy, K. Watanabe, T. Taniguchi, P. Moon, M. Koshino, P. Jarillo-Herrero, and R. C. Ashoori, Science **340**, 1427 (2013).
[24] A. F. Dethlefsen, E. Mariani, H.-P. Tranitz, W. Wegscheider, and R. J. Haug, Phys. Rev. B **74**, 165325 (2006).
[25] See Supplemental Material at http://link.aps.org/supplemental/10.1103/PhysRevLett.121.226801 for additional data and the description of methods and fabrication procedures.
[26] F. Amet, J. R. Williams, K. Watanabe, T. Taniguchi, and D. Goldhaber-Gordon, Phys. Rev. Lett. **110**, 216601 (2013).
[27] R. Geick, C. H. Perry, and G. Rupprecht, Phys. Rev. **146**, 543 (1966).
[28] A. C. Balram, C. Toke, A. Wojs, and J. K. Jain, Phys. Rev. B **91**, 045109 (2015).
[29] A. Schmeller, J. P. Eisenstein, L. N. Pfeiffer, and K. W. West, Phys. Rev. Lett. **75**, 4290 (1995).

[30] R. H. Morf, N. d'Ambrumenil, and S. Das Sarma, Phys. Rev. B **66**, 075408 (2002).
[31] J. K. Jain, Phys. Rev. Lett. **63**, 199 (1989).
[32] S. S. Mandal and J. K. Jain, Phys. Rev. B **63**, 201310 (2001).
[33] U. Wurstbauer, D. Majumder, S. S. Mandal, I. Dujovne, T. D. Rhone, B. S. Dennis, A. F. Rigosi, J. K. Jain, A. Pinczuk, K. W. West, and L. N. Pfeiffer, Phys. Rev. Lett. **107**, 066804 (2011).
[34] A. C. Balram, U. Wurstbauer, A. Wjs, A. Pinczuk, and J. K. Jain, Nat. Commun. **6**, 8981 (2015).
[35] S. Geraedts, M. P. Zaletel, Z. Papi, and R. S. K. Mong, Phys. Rev. B **91**, 205139 (2015).
[36] K. Vyborny, A. F. Dethlefsen, R. J. Haug, and A. Wojs, Phys. Rev. B **80**, 045407 (2009).
[37] J. Alicea and M. P. A. Fisher, Phys. Rev. B **74**, 075422 (2006).
[38] M. Kharitonov, Phys. Rev. B **85**, 155439 (2012).